The 2010 IEEE/RSJ International Conference on
Intelligent Robots and Systems
October 18-22, 2010, Taipei, Taiwan

Stroke plane deviation for a microrobotic fly

Benjamin M. Finio, *Student Member, IEEE*, John P. Whitney and Robert J. Wood, *Member, IEEE*

Abstract— **Wing motion in most flapping-wing micro air vehicles (MAVs) is restricted to a flat stroke plane in order to simplify analysis and mechanism design. An MAV actuation and transmission design capable of controlling flapping motions and deviations from the mean stroke plane using relatively simple modifications to a proven design is presented. This allows preliminary investigation into more power-efficient wing trajectories, an important concern for small MAVs. A theoretical quasi-steady model of flapping wing flight is used to predict wing motions, and these predicted trajectories are compared to empirically observed trajectories from a test device. The ratio of average lift to average aerodynamic power is used as an efficiency metric to compare stroke trajectories.**

I. Introduction

Within the last decade there has been increased interest in the area of flapping-wing micro air vehicles (MAVs) due to potential advantages over fixed-wing vehicles at small scales. Such vehicles range from larger bat and bird-sized ornithopters [1], [2], [3], [4] to smaller insect-sized vehicles and associated components [5], [6], including the Harvard Microrobotic Fly (HMF) [7], [8], [9], and even hybrid mechanical-biological systems [10]. The study of flapping-wing aerodynamics is a relatively new area, as the vast majority of flight vehicle research over the past 100 years has been in fixed or rotary wing aircraft. As such, engineers frequently look to flapping wing animals for design inspiration, especially with regards to morphology and motion. One frequent simplifying assumption is that the stroke plane is flat, i.e. the torsional axis of the wing flaps back and forth in a plane, and does not deviate vertically (Fig. 1 illustrates the wing motion and defines wing angles). There are two reasons for this assumption: (1) many biological wing trajectories do show relatively flat stroke planes, and (2) a flat stroke plane greatly simplifies mechanical construction, as a planar crank-rocker four-bar mechanism with a DC motor (or slider-crank with a linear piezoelectric actuator in the case of the HMF [11]) can be used to generate oscillatory wing motion; whereas stroke-plane deviation requires a more complicated three-dimensional mechanism or a spherical joint (such as the five-bar mechanism with auxiliary four-bar in [12]).

While the flat-stroke plane assumption seems to be a reasonable approximation and has proven successful for several MAV prototypes, inspection of biological data does reveal oval, U-shaped and figure-of-eight wing trajectories [13], [14], [15] (Fig. 2). Recent theoretical fluid dynamics studies of flapping-wing flight have shown that wing trajectories with nonzero stroke plane deviation may be more efficient and effective in terms of the power that must be expended to keep the vehicle aloft or maneuver [16], [17]. Many current MAV designs have limited flight times due to the limited capacity and energy density of available small-scale power supplies [18], and the future of MAV flight depends heavily on improvement of energy sources such as Lithium-polymer batteries. Thus, any potential increase in efficiency is of vital importance. Since all previous HMF designs were restricted to flapping in a flat stroke plane, the investigation of potentially more efficient stroke trajectories involving stroke plane deviation was not possible. The new design presented here enables a preliminary comparison of different trajectory types based on the merits of lift generation and aerodynamic power expenditure as calculated by a theoretical blade-element aerodynamic model. The added complexity and mass associated with such mechanisms is also considered.

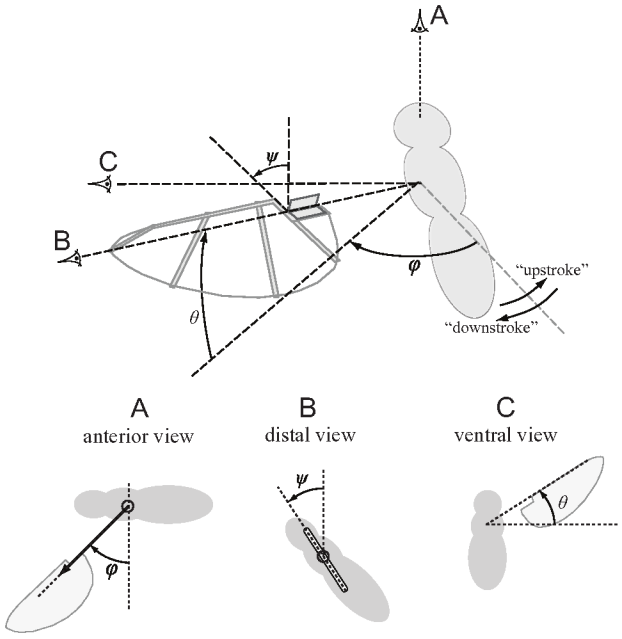

Fig. 1. Definitions of flapping-wing stroke parameters. The angle of rotation of the torsional axis of the wing measured about an axis perpendicular to the mean stroke plane is the *stroke angle* ϕ; the out-of-plane angle measured to the torsional axis of the wing is the *deviation angle* θ; and the rotation of the wing about its torsional axis is the *rotation angle* ψ. The wing flapping forward with respect to the body is referred to as the "downstroke", flapping backward with respect to the body is the "upstroke". Figure not to scale.

The authors are with the School of Engineering and Applied Sciences and the Wyss Institute for Biologically Inspired Engineering, Harvard University, Cambridge, MA 02138 bfinio@fas.harvard.edu

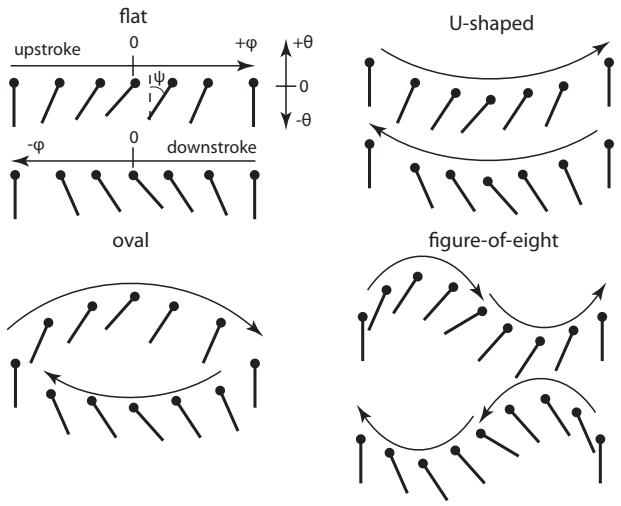

Fig. 2. An "unwrapped" distal view of nominal stroke types. Most MAVs have flat stroke planes, but many more varied trajectories are observed in nature. The filled-in circle represents the leading edge of the wing (assumed to be coincident with the torsional axis for this figure, although this need not be the case). Wing motion is parameterized by the angles ϕ, θ and ψ. For illustration purposes only, not to scale.

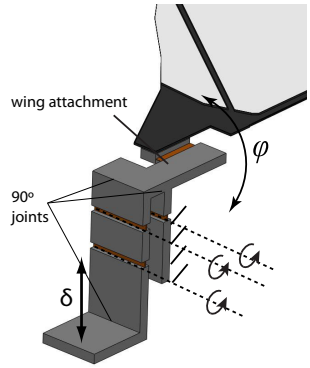

Fig. 3. Illustration of one-half of the original HMF transmission. In this drawing, δ is an actuated input and ϕ is the wing flapping as defined in Fig. 1.

II. Background and Previous Work

Unlike conventional aircraft which utilize control surfaces for decoupled roll, pitch and yaw control (i.e. elevators, ailerons and rudders), insects primarily use asymmetric changes in wing kinematics for attitude control [19] (it has also been shown that insects can use abdominal and leg movements to aid in maneuvering [20], but that is beyond the scope of this work). Insects possess distinct groups of power and control muscles used to generate primary flapping motion and control these asymmetric motions respectively [21], [22], [23], [24]. Previous versions of the HMF have experimented with this idea, using a single large piezoelectric actuator to flap the wings, and smaller actuators to change the kinematics of the four-bar transmission, allowing asymmetric modulation of stroke amplitude [25], [26]. Since stroke-plane deviation angles are typically about an order of magnitude smaller than stroke amplitude (i.e. about 10 degrees compared to 100 degrees peak-to-peak), this also seems like a suitable application for separation of power and control actuators. Using previously developed fabrication techniques [27], a two-input transmission system consisting of two orthogonal flexure-based four-bars for actuation of stroke angle and deviation angle is constructed. Mechanism design, kinematic and dynamic analysis, and experimental results are presented in the following sections.

III. Mechanism Design and Fabrication

The original HMF transmission is a symmetric four-bar that converted a single linear actuator input into rotational motion of two wings. The flexure-based transmission, made from a layered combination of rigid carbon fiber sheets and flexible polymers, is laser-micromachined in two dimensions and then assembled into a three dimensional structure (Fig. 3). Flexures can either be fixed at 90 degrees using an adhesive, or left free to function as revolute joints. Previous modifications of this design to allow stroke amplitude modulation required additional actuator inputs but no topological changes to the transmission [25], [26], however this design does not allow for stroke-plane deviation. It is desired to add a controlled degree of freedom with a rotation axis orthogonal to the ϕ rotation axis, while keeping the structure as simple as possible. This can be accomplished by adding a second flexure-based four-bar orthogonal to the original four-bar (Fig. 4). The two primary benefits of this design are that (a) it does not require any additional 90-degree folds, thus keeping fabrication simple and (b) if the flexures are stiff enough to off-axis loads (off-axis compliance must be considered when designing flexure-based mechanisms [28]), it gives decoupled control of stroke amplitude and deviation angle through two actuator inputs. It also only requires the addition of several linkages that are small relative to the overall structure (including airframe and actuators), so the added mass is negligible. Rotation of the wing remains passive as in the original HMF design, as opposed to previous MAV designs with direct control over both flapping and rotation [29], [30]. While there is still some debate as to the level of active or passive control of insect wing rotation, evidence exists to show that rotation is at least partially, if not wholly passive [31].

IV. Kinematics and Dynamics

A. Kinematics

The kinematics of the four-bar mechanisms can be derived using a pseudo-rigid body model, assuming that all carbon fiber links are rigid and that flexures act as ideal revolute joints. This has been shown previously in [25], and the kinematics are reproduced here. The stroke angle ϕ can be written as a function of actuator input δ_1 and link geometry

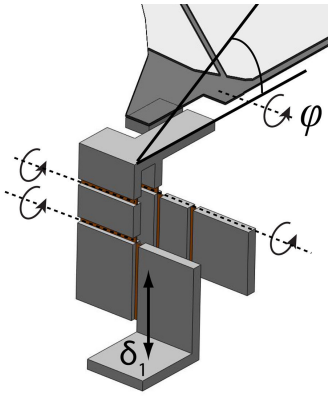

(a)

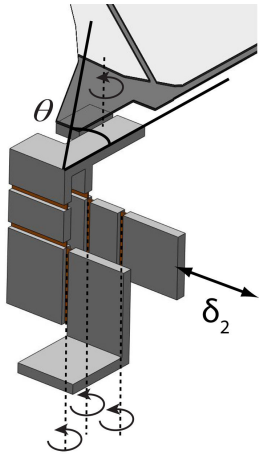

(b)

Fig. 4. Illustration of the stroke plane deviation transmission. Linear actuator inputs δ_1 and δ_2 are converted to (a) stroke angle ϕ and (b) deviation angle θ respectively. Note that this design does not require any additional 90 degree folds than the transmission in Fig. 3.

TABLE I

ACTUATOR DRIVE SIGNALS FOR DIFFERENT STROKE TRAJECTORIES

Trajectory	$\delta_1(t)$	$\delta_2(t)$
Flat	$\frac{A}{T}\sin(\omega t)$	0
Oval	$\frac{A}{T}\sin(\omega t)$	$\frac{B}{T}\sin(\omega t+\frac{\pi}{2})$
figure-of-eight	$\frac{A}{T}\sin(\omega t)$	$\frac{B}{T}\sin(2\omega t)$

L_i (see Fig. 5):

$$L_y = L_1 + L_2 - L_4 \quad (1)$$

$$C_1 = L_3^2 + (L_2 - L_4)^2 - L_1^2 + L_3^2 \quad (2)$$

$$C_2 = 2\sqrt{L_3^2 + (L_2 - L_4)^2} \quad (3)$$

$$\phi = cos^{-1}\left(\frac{(L_y-\delta_1)^2 + C_1}{C_2\sqrt{L_3^2+(L_y-\delta_1)^2}}\right) + tan^{-1}\left(\frac{L_3}{L_y-\delta_1}\right) + tan^{-1}\left(\frac{L_2-L_4}{L_3}\right) - \frac{\pi}{2}. \quad (4)$$

An equivalent formulation can be used to give θ as a function of actuator input δ_2 and the geometry of the second four-bar. Although Eq. 4 is nonlinear, geometry can be selected to give an approximately linear response [8] such that:

$$\phi \equiv T\delta_1 \quad (5)$$

where $T \approx 1/L_3$. Assuming an approximately linear relationship between input displacement and output angle allows the drive signals in Table I to be used to generate the baseline trajectories shown in Fig. 2, where A and B are the desired amplitudes for stroke angle and deviation angle respectively. Actual trajectories in $\phi-\theta$ space are shown in Fig. 6 for given sinusoidal actuator inputs using the full nonlinear kinematics. It is important to note that these trajectories are not perfectly symmetric in ϕ or θ since the transmission kinematics are nonlinear and not symmetric about $\delta_i = 0$.

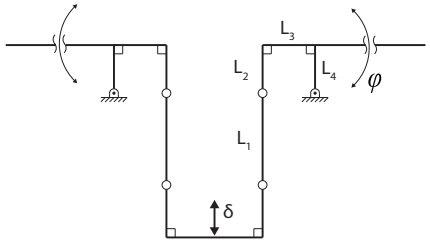

Fig. 5. A pseudo-rigid body model of the original HMF transmission.

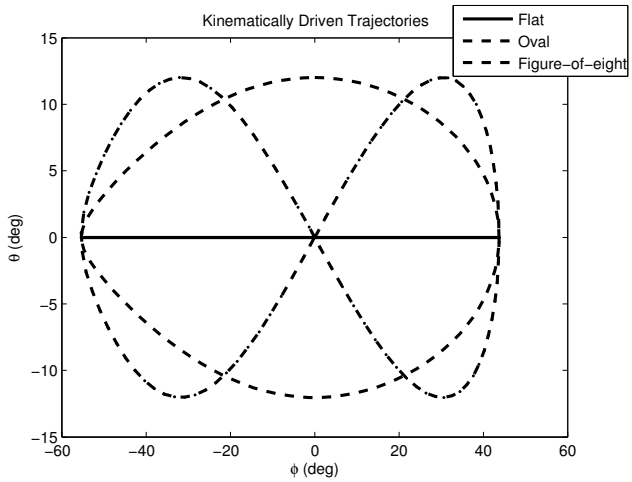

Fig. 6. Wing trajectories using the full nonlinear kinematics, with actuator inputs $\delta_1 = \pm 350\mu m$, $\delta_2 = \pm 100\mu m$, and transmission geometry $L_1 = 500\mu m$, $L_2 = 500\mu m$, $L_3 = 480\mu m$, $L_4 = 500\mu m$ for both the flapping and deviation transmissions.

B. Dynamics

A linearized, lumped parameter dynamic model of the system is shown in Fig. 7. Each of the two actuator/transmission systems acts as a force source in parallel with a spring and damper element, which provide a linear input to a transmission that converts motion to wing rotation. Aerodynamic lift and drag forces (discussed below) act on the wing as the wing moves through a fluid (air). It is important to note that, due

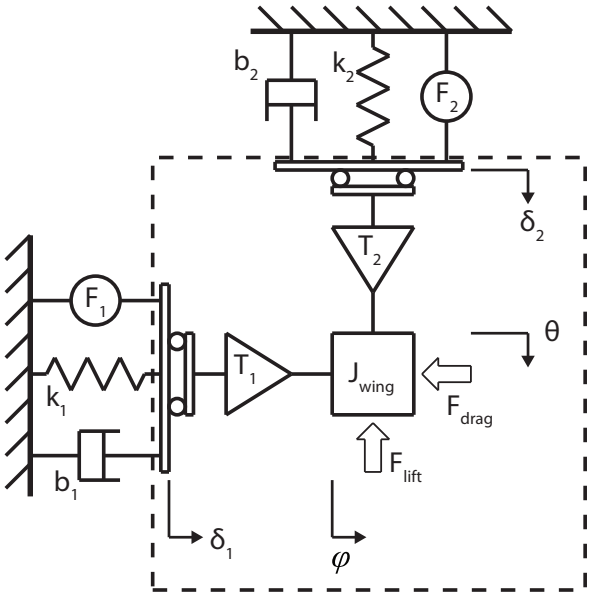

Fig. 7. A schematic of the system dynamic model. Only the subsystem within the dashed box is considered for purposes of this paper. Note that the motions δ_1 and δ_2 are (and therefore ϕ and θ) are kinematically decoupled.

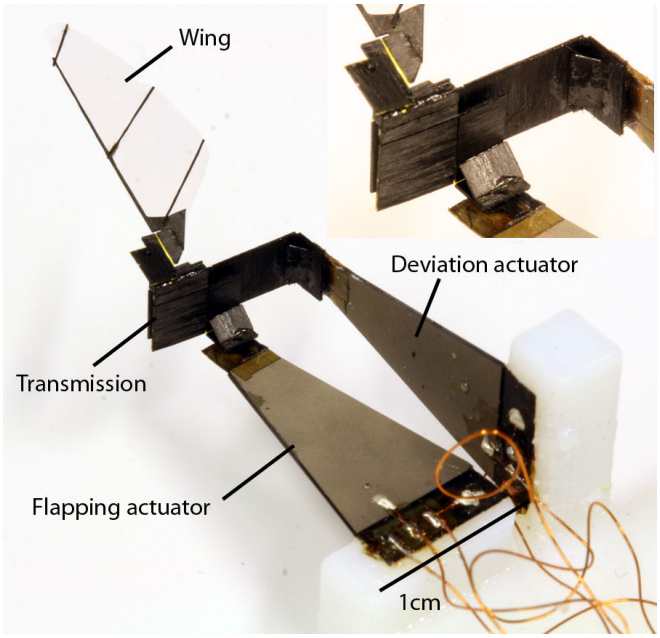

Fig. 8. The test structure used to collect data. Actuator control signals are supplied externally. (inset) A closer view of the transmission.

to the orientation of the flexure hinge that allows the wing to passively rotate, the wing will not passively rotate when only δ_2 is actuated. Actuation of δ_1 is required to generate both lift and drag forces. The model used in this work is only a subsystem of the full dynamic model (inside the dashed box in Fig. 7), equivalent to assuming full kinematic control of δ_1 and δ_2 as control inputs. This allows focus on desired wing trajectories and resulting passive wing rotation. However, while the motions ϕ and θ are *kinematically* decoupled, it will be seen that they are not *dynamically* decoupled since actuation of δ_1 causes a force in the direction of δ_2. While beyond the scope of this work, future dynamic modeling will incorporate the spring-damper elements, with actuators modeled as force, not displacement sources, as well as incorporate feedback control of actuator motion.

The aerodynamic model is a quasi-steady blade element model, meaning that (a) lift and drag forces corresponding to the instantaneous wing velocity (derived empirically in [32]) are used and (b) aerodynamic forces and moments are calculated on thin chordwise strips of the wing, then integrated over the length of the wing to arrive at total forces and moments. Aerodynamic forces and moments are therefore functions of instantaneous wing velocity, angle of attack α (defined as the angle between the local translational velocity vector and the wing chord), and wing geometry. The wing is assumed to be a rigid flat plate attached to a torsional spring on the ψ-axis, rotations about the ϕ and θ axes are driven kinematically. A differential equation for ψ can then be written as a function of inertial, spring and aerodynamic terms and the driving (ϕ, θ) trajectory, of the form

$$\ddot{\psi} = f\left(\phi, \dot{\phi}, \theta, \dot{\theta}, \psi, \dot{\psi}, \mathbf{I}, M\right) \tag{6}$$

where $\mathbf{I}$ is the wing's inertia tensor and M is the term including aerodynamic moments, which are functions of both normal and tangential force coefficients, wing geometry, and proportional to the square of wing velocity and rotation rate. The normal and tangential force coefficients C_N and C_T themselves are functions of α, thus the moment terms are of the form

$$M = f\left(C_N(\alpha), C_T(\alpha), \dot{\phi}^2, \dot{\theta}^2, \dot{\psi}^2, y(r), c(r)\right) \tag{7}$$

where $y(r)$ and $c(r)$ define the position of the leading edge and chord length of the wing as a function of radial position, thus fully defining the planar wing shape. The the reader is referred to [33] for detailed derivation and explanation of the exact form and individual terms in Eqs. 6 and 7.

V. Experiment

A. Methods

A test device using the transmission shown in Fig. 4 with two externally powered piezoelectric actuators and a wing connected to the output link was constructed (Fig. 8). Note that on-board power supply and electronics for the HMF are ongoing research areas [34], [35], but not considered for the tests presented here. Piezoelectric actuators were driven with a custom Matlab program (Mathworks Inc.). 0-5V range analog signals output from the computer were amplified to levels required to drive the actuators (200-300V) with a high-voltage amplifier (Trek Inc.). Wing motion was filmed using two Phantom V7.3 high-speed cameras (Vision

Research) oriented at approximately 90° to each other. Two-dimensional coordinates of points on the wing were extracted from the left and right camera views separately using 2D motion tracking software (ProAnalyst from Xcitex Inc.). The use of two cameras allowed stereoscopic reconstruction of full three-dimensional wing kinematics [36]. Note that the calibration procedure calculates the relative camera positions and orientations, so the camera positions need not be exactly known *a priori*. Still images from two sample videos are shown in Fig. 9.

B. Results

Three trajectory types are tested: flat, oval, and figure-of-eight. Trajectories are driven open-loop with the actuator signals presented in Table I. For each trajectory type, the wing angles ϕ, θ and ψ are plotted as functions of time in Figure 11, however visualizing the shape of each trajectory is easier when viewing a plot of θ vs. ϕ (Fig. 10). One can imagine this as approximately the wingtip trajectory that would be seen with an edge-on view of the wing mapped from the surface of a sphere.

It is immediately evident from Fig. 10 that when driven at high frequencies, the wing trajectories do not match those predicted from kinematics (Fig. 2). However, when driven at low frequencies - i.e. when aerodynamic and inertial forces are negligible - reasonable flat, oval and figure-of-eight trajectories can be obtained (Fig. 10b,c,e). There are two possible sources of error. First, the compliance of the stroke-plane-deviation actuator and transmission (k_2 in Fig. 7) allows undesired vertical motions of the wing due to coupling of the lift force, as there is no feedback system in place to reject disturbances in this direction. Second, the transmission design relies heavily on the idea that flexure joints will act as ideal revolute joints, with one axis of rotation and infinite off-axis stiffness. In practice this is not true [28], and off-axis compliance of the flexure joints can lead to undesired motion. Future revisions of the design will address both of these issues.

Despite the fact that the observed trajectories are not as consistent as hoped, experimental results can still be compared to the aerodynamic model in [33] in order to make a preliminary comparison of efficiency. The model takes the time history of ϕ and θ as inputs and calculates expected passive rotation ψ and resulting average aerodynamic lift and power. Fig. 11 shows experimental and predicted passive rotation for the recorded flapping and deviation kinematics. Average lift, average aerodynamic power, and lift/power (all theoretical values, as lift and aerodynamic power are not measured directly) as a measure of efficiency are compared for each trajectory (Table II). Despite having the largest value of average lift, the flat trajectory consumes more power and thus has a lift/power ratio roughly the same as the oval trajectory. The figure-of-eight, while it has the lowest lift value, also has the lowest aerodynamic power and therefore the combination of these two terms gives it the best lift/power ratio. However, the data presented here is preliminary and *not* conclusive enough to make the claim that a figure-of-eight stroke is more efficient under all circumstances. Further testing on a larger number of stroke trajectories is required. Automation of testing and data collection, i.e. automatically generating actuator drive signals, collecting force data, extracting wing kinematics, and measuring actuator power consumption will allow a significant increase in the amount of data that can be collected.

TABLE II

THEORETICAL AERODYNAMIC LIFT, POWER AND EFFICIENCY FOR THREE OBSERVED WING TRAJECTORIES

Stroke	Avg. Lift (mN)	Avg. Power (mW)	Lift/Power (N/W)
Flat	2.7	23.2	.12
Oval	1.59	14.0	.11
Fig. 8	1.54	10.4	.15

VI. CONCLUSIONS

The work presented here is intended as a preliminary exploration into actuated stroke-plane deviation for flapping-wing MAVs, specifically the Harvard Microrobotic Fly, since the vast majority of MAVs utilize flat stroke planes. While investigated here due to potential gains in efficiency over a flat stroke, stroke plane deviation also has promise for vehicle maneuvering and stability, and this will be the subject of future work. The authors do *not* make the claim that a given trajectory type is more efficient than another based on the preliminary results presented here. Much further work, both theoretical and experimental, will be required to make any claim of an optimal trajectory. Most aerodynamic studies, such as [17] and [33] assume kinematic control of wing flapping and deviation, without considering actuator or transmission dynamics. While the device presented here can achieve direct kinematic control of wing trajectory at low frequencies with no feedback system in place, results at high frequencies show that actuator/transmission dynamics and compliance play a vital role in resultant trajectories and cannot be neglected. Future work will include actuator position feedback in order to follow kinematically predetermined trajectories. Additional experimental measurements may also be made to further evaluate the lift/power criteria. Lift force can be measured directly as in [33], [37] and compared to theoretical values. While it is difficult to experimentally measure aerodynamic power, electrical power input to the actuators can be measured directly and used as a criteria. Additional work in all of these areas will allow development of wing trajectories and thorax designs for increased maneuverability and flight times of insect-sized MAVs.

VII. ACKNOWLEDGEMENTS

This work was supported in part by the Army Research Laboratory (award number W911NF-08-2-0004) and an ND-SEG graduate fellowship (Ben Finio).

REFERENCES

[1] J. Park and K. Yoon, "Designing a Biomimetic Ornithopter Capable of Sustained and Controlled Flight," *Journal of Bionic Engineering*, vol. 5, no. 1, pp. 39–47, 2008.

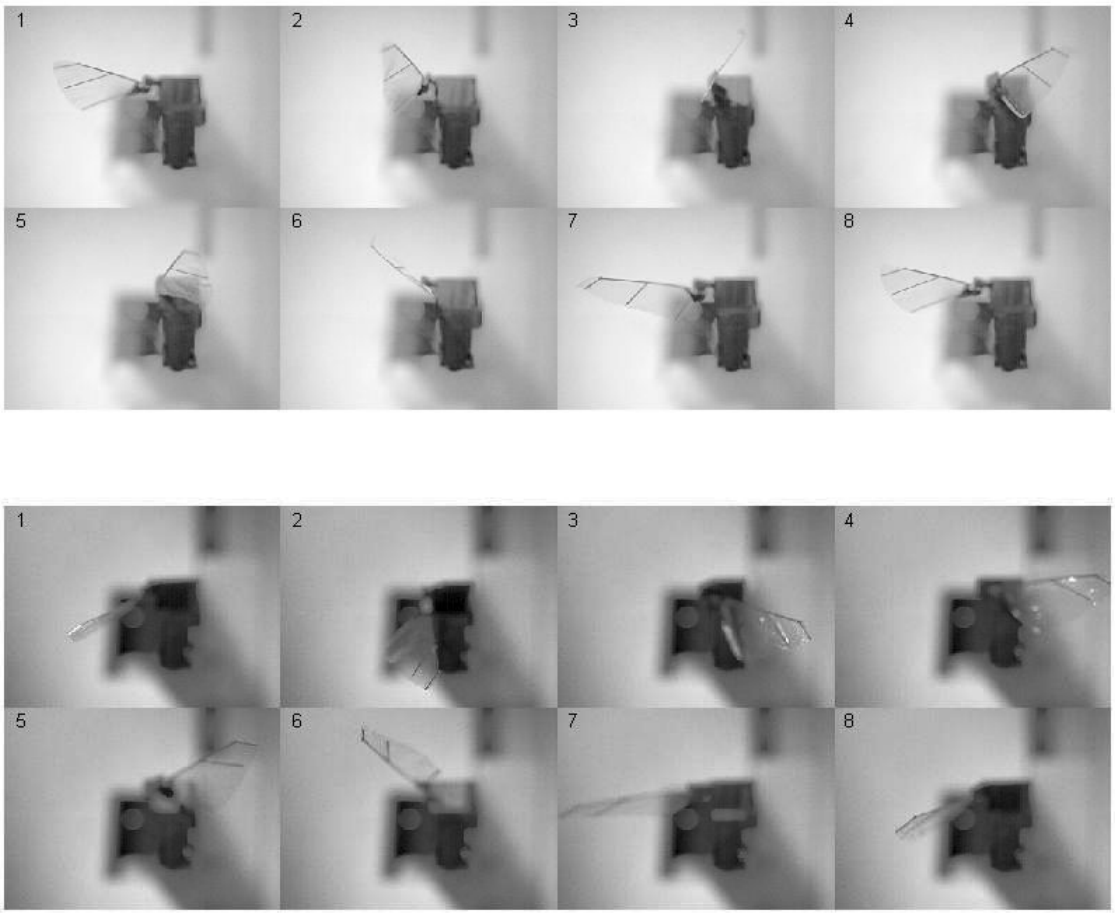

Fig. 9. Still images from one camera for flat (top) and oval (bottom) stroke trajectories. Data was recorded at 5000fps, so 50 data points were collected per cycle flapping at 100Hz. Every 7th frame for one cycle is shown, the time between images is 1.4msec.

[2] G. Bunget and S. Seelecke, "BATMAV: a biologically-inspired micro-air vehicle for flapping flight: kinematics and actuation," in *Proceedings of SPIE*, vol. 6928. SPIE, 2008, p. 69282F.

[3] T. Pornsin-Sirirak, Y. Tai, C. Ho, and M. Keennon, "Microbat: A Palm-Sized Electrically Powered Ornithopter," *Proceedings of NASA/JPL Workshop on Biomorphic Robotics*, pp. 14–17, 2001.

[4] F. Van Breugel, W. Regan, and H. Lipson, "Demonstration of a Passively Stable, Untethered Flapping-Hovering Micro-Air Vehicle," *IEEE Robotics & Automation Magazine*, p. 69, 2008.

[5] Y. Kawamura, S. Souda, S. Nishimoto, and C. Ellington, "Clapping-wing Micro Air Vehicle of Insect Size," *Bio-mechanisms of Swimming and Flying*, pp. 319–330, 2008.

[6] E. Wetzel, R. Polcawich, C. Kroninger, J. Pulskamp, and J. Bronson, "Bio-Mimetic Millimeter-Scale Flapping Wings for Micro Air Vehicles," 2009.

[7] R. Wood, "Liftoff of a 60mg flapping-wing MAV," in *IEEE/RSJ International Conference on Intelligent Robots and Systems*, 2007, pp. 1889–1894.

[8] ——, "Design, fabrication, and analysis, of a 3DOF, 3cm flapping-wing mav," pp. 1576–1581, 2007.

[9] ——, "The first takeoff of a biologically inspired at-scale robotic insect," in *IEEE Transactions on Robotics*, vol. 24, no. 2, 2008, pp. 341–347.

[10] S. Pulla and A. Lal, "Insect powered micro air vehicles," in *IEEE International Conference on Robotics and Automation*. IEEE Press, 2009, pp. 4414–4419.

[11] R. Wood, E. Steltz, and R. Fearing, "Optimal energy density piezoelectric bending actuators," *Sensors and Actuators A: Physical*, vol. A 119, pp. 476–488, 2005.

[12] S. Banala and S. Agrawal, "Design and optimization of a mechanism for out-of-plane insect winglike motion with twist," *Journal of Mechanical Design*, vol. 127, p. 841, 2005.

[13] S. Fry and M. Dickinson, "The aerodynamics of free-flight maneuvers in drosophila." *SCIENCE*, vol. 300, no. 5618, pp. 495–498, 2003.

[14] T. Maxworthy, "The fluid dynamics of insect flight," *Annual Review of Fluid Mechanics*, vol. 13, no. 1, pp. 329–350, 1981.

[15] C. Ellington, "The aerodynamics of hovering insect flight. III. Kinematics," *Philosophical Transactions B*, vol. 305, no. 1122, p. 41, 1984.

[16] H. Dong, Z. Liang, and M. Harff, "Optimal Settings of Aerodynamic Performance Parameters in Hovering Flight," *International Journal of Micro Air Vehicles*, vol. 1, no. 3, pp. 173–181, 2009.

[17] G. Berman and Z. Wang, "Energy-minimizing kinematics in hovering insect flight," *Journal of Fluid Mechanics*, vol. 582, pp. 153–168, 2007.

[18] M. Karpelson, P. Whitney, G. Wei, and R. Wood, "Energetics of Flapping-Wing Robotic Insects: Towards Autonomous Hovering Flight," in *IEEE/RSJ International Conference on Intelligent Robots and Systems*, 2010, in press.

[19] G. K. Taylor, "Mechanics and aerodynamics of insect flight control," *Biological Reviews*, vol. 76, no. 04, pp. 449–471, 2001.

[20] Stacey Combes, 2010, personal communication.

[21] M. Dickinson and M. Tu, "The function of dipteran flight muscle," *Comp. Biochem. Physiol.*, vol. 116A, no. 3, pp. 223–238, 1997.

[22] C. Balint and M. Dickinson, "The correlation between wing kinematics and steering muscle activity in the blowfly Calliphora vicina," *Journal of Experimental Biology*, vol. 204, no. 24, p. 4213, 2001.

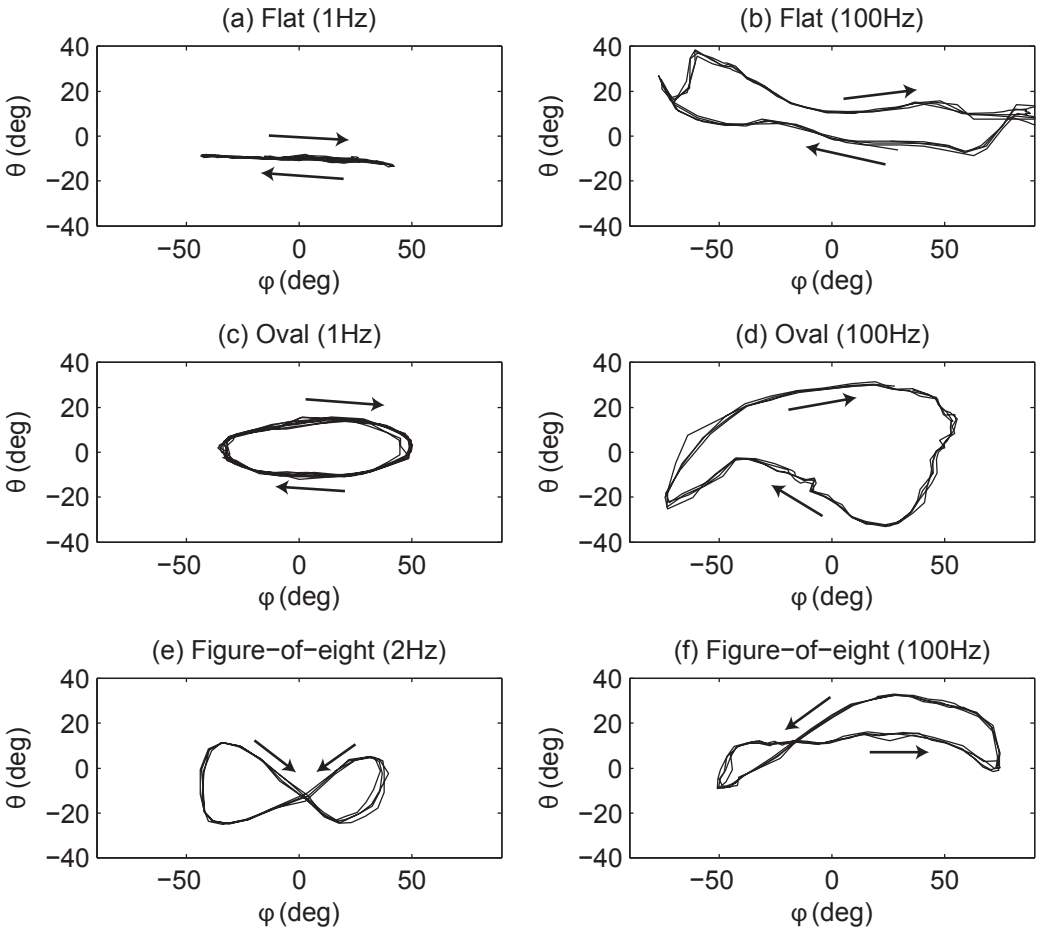

Fig. 10. θ vs ϕ for flat , oval and figure-of-eight trajectories at high and low frequencies. Actuation at low frequencies can achieve kinematically predetermined wing trajectories (left column), while actuation at higher frequencies appears to excite oscillations in the stroke plane deviation direction (right column). Direction of motion is indicated with arrows.

[23] ——, "Neuromuscular control of aerodynamic forces and moments in the blowfly, Calliphora vicina," *Journal of Experimental Biology*, vol. 207, no. 22, p. 3813, 2004.

[24] R. Dudley, *The biomechanics of insect flight: form, function, evolution*. Princeton University Press, 2000.

[25] B. Finio, J. Shang, and R. Wood, "Body Torque Modulation for a Microrobotic Fly," in *IEEE International Conference on Robotics and Automation*, 2009, pp. 3449–3456.

[26] B. Finio, B. Eum, C. Oland, and R. Wood, "Asymmetric flapping for a robotic fly using a hybrid power-control actuator," in *IEEE/RSJ International Conference on Intelligent Robots and Systems*, 2009, pp. 2755–2762.

[27] R. Wood, S. Avadhanula, R. Sahai, E. Steltz, and R. Fearing, "Microrobot Design Using Fiber Reinforced Composites," *Journal of Mechanical Design*, vol. 130, pp. 52 304–52 315, 2008.

[28] A. Hoover and R. Fearing, "Analysis of off-axis performance of compliant mechanisms with applications to mobile millirobot design," in *IEEE/RSJ International Conference on Intelligent Robots and Systems*, 2009, pp. 2770–2776.

[29] R. Fearing, K. Chiang, M. Dickinson, D. Pick, M. Sitti, and J. Yan, "Wing transmission for a micromechanical flying insect," in *IEEE International Conference on Robotics and Automation*, vol. 2, 2000, pp. 1509–1516.

[30] M. Sitti, "PZT actuated four-bar mechanism with two flexible links for micromechanical flying insect thorax," in *IEEE International Conference on Robotics and Automation*, vol. 4, 2001, pp. 3893–3900.

[31] A. Bergou, S. Xu, and Z. Wang, "Passive wing pitch reversal in insect flight," *J. Fluid Mech.*, vol. 591, pp. 321–337, 2007.

[32] M. Dickinson, F. Lehmann, and S. Sane, "Wing rotation and the aerodynamic basis of insect flight," *Science*, vol. 284, no. 5422, pp. 1954–1960, 1999.

[33] J. Whitney and R. Wood, "Aeromechanics of Passive Rotation in Flapping Flight," *Journal of Fluid Mechanics*, 2010, in press.

[34] M. Karpelson, G. Wei, and R. Wood, "A review of actuation and power electronics options for flapping-wing robotic insects," in *IEEE International Conference on Robotics and Automation*, 2008, pp. 779–786.

[35] ——, "Milligram-Scale High-Voltage Power Electronics for Piezoelectric Microrobots," in *IEEE International Conference on Robotics and Automation*, 2009.

[36] J. Bouget, "Camera Calibration Toolbox for Matlab," 2008, `www.vision.caltech.edu/bouguetj/calib_doc/`

[37] R. Wood, K. Cho, and K. Hoffman, "A Novel Multi-Axis Force Sensor for Microrobotics Applications," *J. Smart Materials and Structures*, 2009.

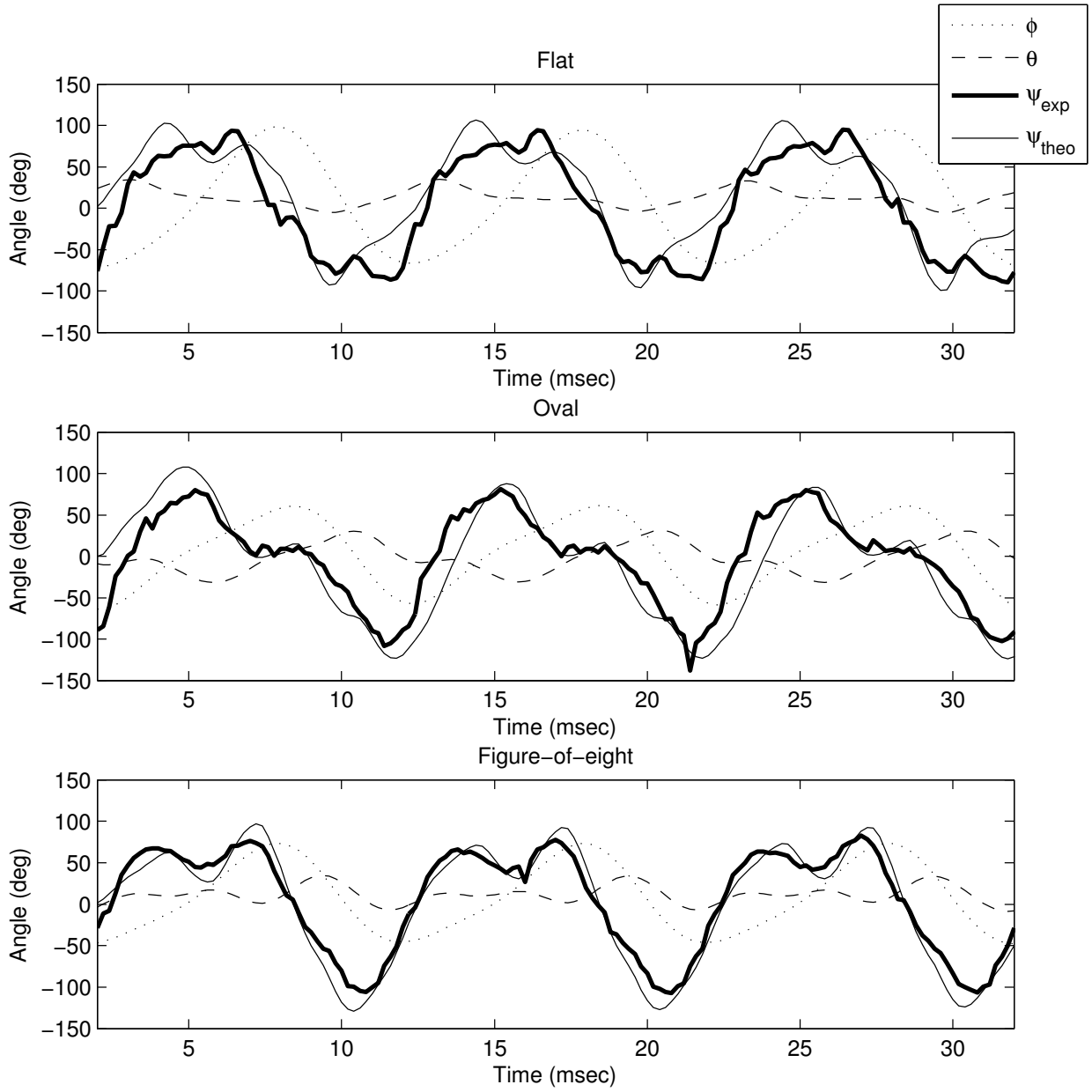

Fig. 11. Experimental flapping and deviation angles ϕ and θ plotted with experimental and theoretical rotation angles ψ_{exp} and ψ_{theo}; for flat, oval and figure-of-eight wingstrokes. There is good agreement between observed and prediction passive wing rotation.